Chalcogenide Letters Vol. 22, No. 5, May 2025, p. 481 - 491

Influence of Ag content on direct current conductivity of $Ag_x(As_2(Te_{0.5}Se_{0.5})_3)_{100-x}$ system

G. R. Štrbac [a,*], O. Bošák [b], D. Štrbac [c], R. Vigi [a], M. Kubliha [b], S. Minárik [b]
[a] *University of Novi Sad, Faculty of Sciences, Department of Physics, Trg D. Obradovića 4, 21000 Novi Sad, Serbia*
[b] *Slovak University of Technology, Faculty of Materials Science and Technology, Bottova 25, 91724 Trnava, Slovakia*
[c] *University of Novi Sad, Faculty of Technical Sciences, Trg D. Obradovića 6, 21000 Novi Sad, Serbia*

The temperature dependence of direct current (DC) conductivity, silver content, and the presence of crystalline phases in amorphous and annealed chalcogenides from the $Ag_x(As_2(Te_{0.5}Se_{0.5})_3)_{100-x}$ system was investigated. Amorphous samples exhibited semiconducting behavior, with conductivity increase as the silver content raised. This increase was primarily attributed to electron transitions into delocalized states from states localized near the Fermi level. Percolation behavior in conductivity was observed in the samples containing 7 at.% or more silver. For annealed samples with silver content below 9 at.%, temperature-independent DC conductivity was identified, accompanied by a decrease in conductivity as the silver content increased.

(Received February 12, 2025; Accepted May 22, 2025)

Keywords: Amorphous materials, Conductivity, Band gap, Silver doping, Percolation transition

1. Introduction

Vitreous semiconductors have been extensively studied for their diverse range of potential applications [1]. These materials have proven valuable in areas such as infrared optical components, infrared laser power transmission, sensors, detectors, phase-change memory devices, photolithography, thermal imaging, infrared spectroscopy, and photovoltaic technologies. Their utility is further enhanced by characteristics such as the lack of long-range order, high non-linear optical properties, and enhanced stability and durability. [2-17]. A distinct advantage of these materials lies in the ability to precisely tune their properties through adjustments in composition, alloying, and synthesis conditions, enabling tailored solutions for specific technological needs.

In recent years, interest in studying the conductivity of chalcogenide glasses (ChGs) has grown significantly due to their potential applications in electronic devices [18-21]. However, the very low electrical conductivity of undoped vitreous chalcogenides poses a challenge for both electrical measurements and applications. A highly effective approach to overcoming this limitation is doping these amorphous semiconductors with transition metals. This modification not only improves electrical transport but also enhances other physical properties, including optical and electrical characteristics, making them more suitable for advanced applications.

The behavior of a material depends on its composition, the matrix used, the element interacting with the matrix, and its structural properties. Additionally, the uniformity of chalcogenide glass is crucial in influencing its electrical properties. In glasses doped with a higher atomic percentage of silver, phase separation and inhomogeneity are common, leading to structural non-uniformities. These factors can explain the abrupt fluctuations in electrical conductivity observed in certain silver-doped glasses. Phase separation usually happens as the system aims to minimize its free energy, leading to a structure that deviates from a fully polymerized network

* Corresponding author: grstrbac@uns.ac.rs
https://doi.org/10.15251/CL.2025.225.481

with extensive interconnectivity, which would otherwise have high free energy. The amorphous matrix reduces free energy by separating into distinct phases.

Conductivity in chalcogenide glasses (ChGs) is typically achieved through silver (Ag) doping, although it can be influenced by various compositional factors [21]. When doped with metals like silver, these glasses may exhibit either mixed ionic-electronic or purely ionic conductivity. The transition to ionic conduction is governed by the total metal content, the uniformity of the glass structure, and the particular chalcogen element present. Higher levels of Ag doping have been observed to enhance conductivity in stoichiometric As-based chalcogenide glasses [22].

Additionally, the composition of the glass matrix and the relative amount of arsenic to chalcogen have been shown to greatly impact the conductivity of chalcogenide glasses doped with silver [22-24]. Studies on amorphous $Ag_x(As_{0.33}Ch_{0.67})_{100-x}$ (where Ch represents S, Se, or Te) have highlighted a relationship between their electrical properties and microstructure, as well as the substitution of chalcogen atoms. A decrease in ionic conductivity has been observed if sulfur is substituted with selenium or tellurium. Furthermore, it is found that phase separation into silver-rich and silver-poor regions influences the conductivity, driving the transition from semiconductor to ionic conductor in sulfur- and selenium-based glasses [22].

The variation in conductivity of $Ag_x(As_{0.33}S_{0.67})_{100-x}$ takes place between 7 and 8 at.% Ag resulting from the volume percolation of a highly conductive, silver-rich phase with a composition close to $AgAsS_2$ [25]. In the range of 8-26 at.% Ag, conductivity is primarily ionic, as confirmed by impedance spectroscopy, with residual electronic conductivity being minimal [26].

A similar percolation behavior is observed in the $Ag_x(As_{0.33}Se_{0.67})_{100-x}$ glass when the silver proportion reaches 6 at.% [22]. Although the conductivity transforms from electronic to ionic, it still remains a mixed ionic-electronic system, with a significant electronic share in the high silver concentration range [22].

In contrast, the $Ag_x(As_{0.33}Se_{0.335}Te_{0.335})_{100-x}$ glass does not exhibit percolation behavior. Instead, its conductivity is primarily electronic throughout its composition range [22].

To better understand the composition of chalcogenide glasses and their potential applications, particularly as semiconductor materials, it is essential to investigate their electrical characteristics. This study focuses on evaluating the direct current (DC) conductivity of chalcogenides with an $As_{40}Te_{30}Se_{30}$ matrix, doped with varying silver concentrations ranging from 1 to 17 at.%. The aim is to explore how silver doping influences the electrical properties and overall structure of this glass system.

2. Experimental

Using a well-established melt-quench method, bulk glass materials were synthesized. High-purity elements (p.a.) were weighed based on their atomic percentages in the desired glass composition. These elements were loaded into silica tubes, which were then vacuum-sealed. The sealed tubes were heated in a furnace, following a programmed temperature profile that gradually reached a maximum of 950°C. During heating, the sample was periodically agitated to ensure uniform mixing. The temperature was held at 950°C for 12 hours. Afterward, the sample was air-quenched, as the As-Se-Te matrix is known to form highly stable glasses, eliminating the need for water quenching. This process yielded high-quality glass material. For electrical measurements, the bulk glasses were polished into plan-parallel prisms with dimensions of approximately 10 × 10 × 1.5 mm.

SEM measurements were conducted on a JEOL JSM 7600F scanning electron microscope with an energy-dispersive spectrometer (EDS), with 20 kV acceleration voltages. Before analysis, each sample was coated with a thin gold layer.

Samples for electrical and dielectric property measurements were prepared as plan-parallel rectangular plates, with a conductive graphite layer applied to contact surfaces. DC conductivity was measured using a Keithley 6517B picoammeter, while 10 V voltage was supplied by the Novocontrol Concept 90 instrument. Measurements were conducted in a nitrogen flow over a temperature range from 0 °C to 30 °C below the glass transition temperature (T_g), with a heating

rate of 5 °C/min and a temperature accuracy of ±1 °C. Each measurement was repeated consecutively without removing the samples, ensuring the apparatus remained under a protective atmosphere. The accuracy of DC measurements is estimated to be around ±2.5%.

3. Results and discussion

SEM and EDS analyses of the surface morphology and sample composition revealed several notable features. Distinct differences in the appearance of annealed and amorphous samples were observed. SEM images clearly showed that amorphous samples exhibited a homogeneous surface with visible shell-like fractures, indicative of residual stress after synthesis - a typical characteristic of glasses. In contrast, the annealed samples displayed a rough and inhomogeneous surface. For example, Figure 1 shows SEM images of the surface of the sample with 13 at.% silver.

Another significant difference was noted in the elemental distribution between amorphous and annealed samples. For amorphous samples, as previously examined [27], area scans showed the existence of silver in the expected percentages. On the other hand, deviations in the As and Se content were observed due to their closeness in the periodic table, which limits the technique in accurately distinguishing them.

In annealed samples with higher silver content, a notable discrepancy between the programmed and actual silver proportions in the surface layer was detected. In the composition with 13 at.% silver, the surface layer showed 20 at.% silver, while in the 17 at.% silver composition, this increased to 24 at.%, with localized areas reaching up to 29 at.%. This indicates significant inhomogeneity and deviations from the intended composition across the investigated sample surfaces.

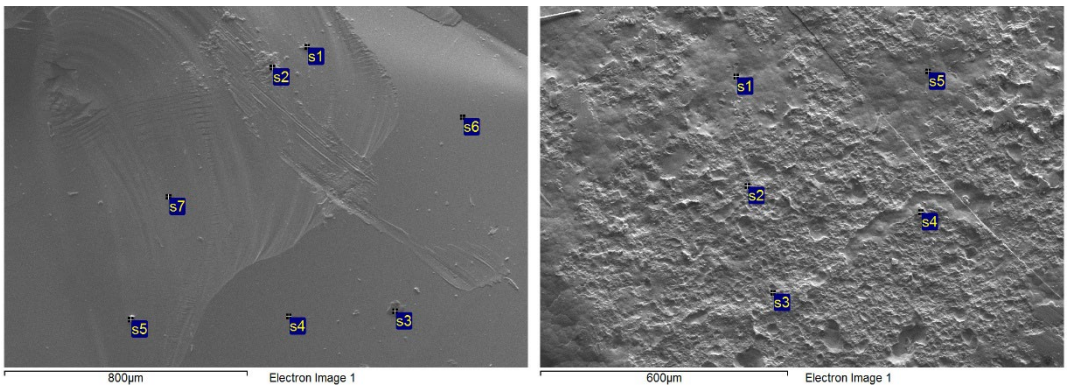

Fig. 1. SEM images of amorphous (left) and annealed (right) sample with 13 at.% of silver.

SEM analysis revealed that both amorphous and annealed samples with 0 and 1 at.% silver exhibited surface regions characterized by small bubbles with thin walls, composed of As_2Se_3 structural units. In the sample with 1 at.% silver, these regions appeared much smaller and more isolated compared to the broader matrix. Figure 2 illustrates the surface morphology of amorphous and annealed samples containing 1 at.% silver, providing a visual example of these observations. Notably, as the silver content increases further, these bubble-like regions disappear entirely. The final results will show that in samples with a low silver content, phase separation does not occur within the sample volume.

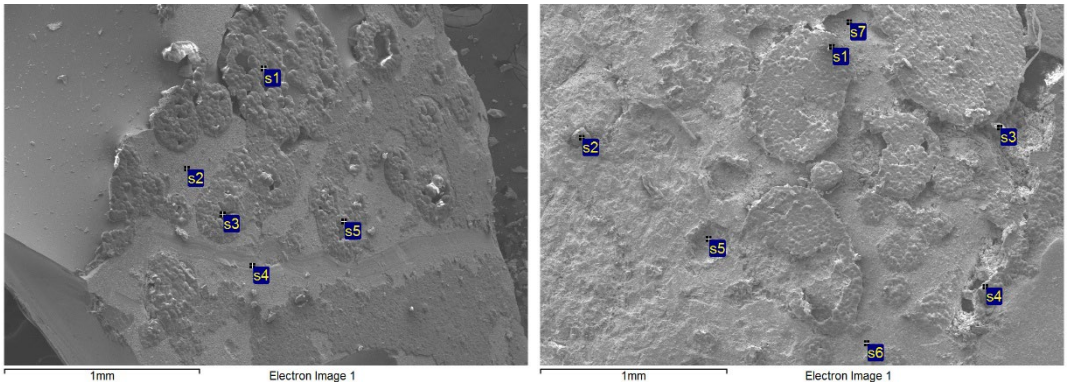

Fig. 2. SEM images of amorphous (left) and annealed (right) sample with 1 at.% of silver

Figure 3a illustrates the direct current (DC) conductivity vs temperature for all synthesized amorphous samples doped with silver. Clearly, the conductivity increases with the silver content, reaching a peak at 17 at.% silver. This can be attributed to the formation and increased proportion of silver-containing structural units, considering the high conductivity of pure silver. The exponential rise in conductivity with temperature, as shown in Figure 3a, indicates the semiconducting nature of the material. For a clearer visual representation of how conductivity changes with both silver content and temperature, Figure 3b presents a contour color fill graph. Notably, significant changes in DC conductivity occur primarily at higher temperatures and with compositions containing higher silver proportions.

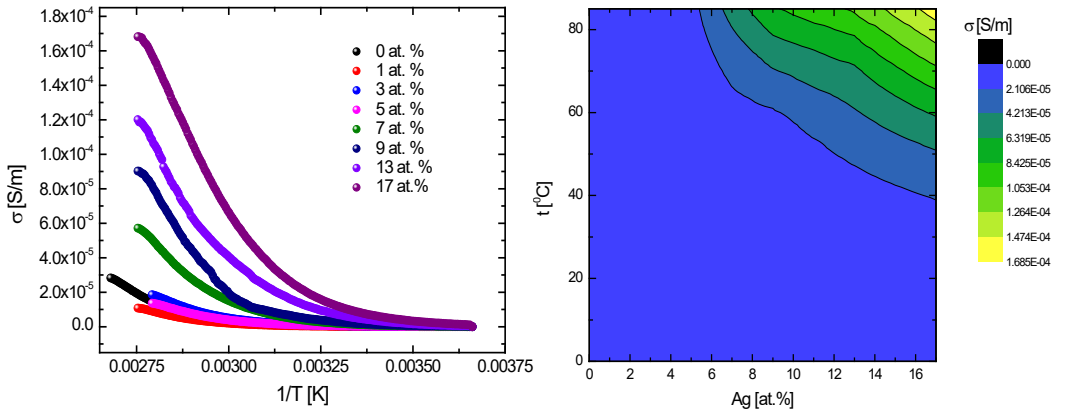

Fig. 3. (a) DC conductivity in amorphous samples in function 1000/T (b) contour colour fill graph changes in conductivity with increasing temperature and the proportion of silver in the composition

Figure 4 shows the dependence of conductivity on the increasing silver content at temperatures of 293 K, 223 K, and 353 K. The lines in the graph serve as guides for the eye.

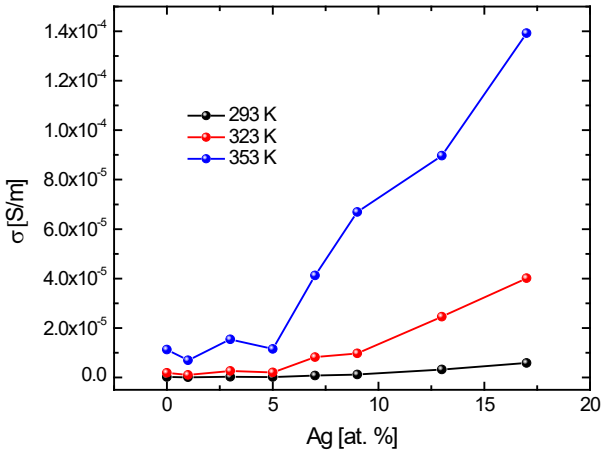

Fig. 4. Dependence of the change in conductivity on the silver content in the composition.

No significant changes in conductivity are observed for compositions with low silver content, up to 5 at.% silver. However, a sharp increase in conductivity is observed starting at 7 at.% silver, and the conductivity jumps become more pronounced with higher temperatures. This indicates that the composition with 5 at.% silver marks a critical point in the conductivity process. At this concentration, the glasses exhibit amorphous semiconductor behavior with electronic conductivity. The percolation behavior of conductivity appears in the $Ag_x(As_2(Te_{0.5}Se_{0.5})_3)_{100-x}$ composition once the silver content reaches 7 at.%. The rapid increase in conductivity can be attributed to a mixed ionic-electronic conductivity, with a significant electronic contribution. This indicates a phase separation into silver-rich and silver-poor regions in the samples, with structures on the order of several microns.

An identical trend was observed in the thermal characteristics of the glasses tested [27]. Specifically, it was found that increasing the silver content beyond 5 at.% leads to changes in the glass-transition temperature, activation energy of the softening process, fluctuation-free volume fraction, and other parameters. Based on the XRD patterns these changes are explained as consequences of structural modifications. Beyond 5 at.% silver, the dominance of $AgAsSe_2$ structural units becomes more pronounced, with only minor structural changes thereafter. The matrix consists of As_2Se_3 and $AsSe_{0.5}Te_{0.5}$ units, along with $AgAsSe_2$. A gradual decrease in the matrix structural units occurs as the silver content increases, while the intensity of peaks corresponding to the $AgAsSe_2$ unit increases significantly. Silver-containing structural units are first detected at 3 at.% silver, and at 5 at.% silver, the matrix units are still present, though the $AgAsSe_2$ units continue to grow. With higher silver concentrations, the matrix structural units disappear, and $AgAsSe_2$ becomes dominant [27]. This shift in structure can be correlated with the observed conductivity jump.

For the composition $Ag_{17}(As_2(Te_{0.5}Se_{0.5})_3)_{83}$, X-ray scans revealed crystalline centers of the $AgAsSe_2$ type [27], which exhibit conductivity several orders of magnitude higher than the glassy analogs [28]. Still, these crystalline centers were not present in the composition with 13 at.% Ag. Although the crystalline centers could potentially influence the mechanism of conductivity, their presence did not significantly influence the electrical measurement results.

The electrical conductivity increase with higher silver content is probably a result of phase separation, specifically the formation of silver-rich regions. This phase separation effect on conductivity enhancement has been observed in other chalcogenide glass (ChG) systems, such as Ag-As-S [25], Ag-As-S-Se [22], and Ag-As-Se [29]. In the case of the $Ag_x(As_{0.33}Se_{0.335}Te_{0.335})_{100-x}$ system, silver atoms were homogeneously incorporated into the $As_{33}Se_{33.5}Te_{33.5}$ matrix, facilitating electronic transfer without any detectable ionic contribution to the overall conductivity [22]. Similarly, in the analogous composition examined in this study, which replaces Te with S in the same atomic proportions, a shift in electrical conductivity behavior was observed around the 5 at.% silver composition [30].

The direct current conductivity increases exponentially with temperature, following the Arrhenius equation, which indicates thermally activated conduction. By analyzing the linear portion of the conductivity versus 1/T plot, the activation energy can be determined from the Arrhenius dependence.

$$\sigma = \sigma_0 e^{\frac{-E_a}{kT}}$$

E_a represents the conduction activation energy, and σ₀ is the pre-exponential factor. The result of linearization of the upper relationship to determine the activation energy and pre-exponential factor is illustrated in Figure 5, with the corresponding values provided in Table 1.

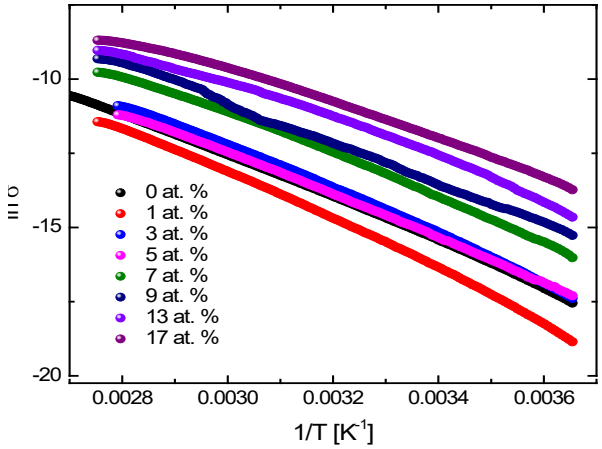

Fig. 5. Dependence of ln σ on 1/T for chalcogenide glasses from the $Ag_x(As_2(Te_{0.5}Se_{0.5})_3)_{100-x}$ system

Table 1. Dependence of pre-exponential factor (σ_0), energy of activation of electrical conductivity (E_a) and conductivity at 85 ^{0}C (σ_{85}).

Ag [at.%]	σ_0 [S/m]	σ_{85} [10^{-5}S/m]	E_a [eV]
0	7759.1(11)	1.4678	0.6194(16)
1	75482.2(11)	0.90622	0.701(3)
3	27802.3(11)	1.8518	0.6456(24)
5	8063.1(11)	1.3644	0.6176(16)
7	17207.9(11)	5.0708	0.602(3)
9	14236.6(11)	8.2007	0.5856(16)
13	3314.3(12)	10.835	0.526(4)
17	1520.6(11)	15.751	0.490(3)

Figure 6 shows the dependence of the activation energy (Figure 6a) and the pre-exponential factor (Figure 6b) on the proportion of silver in the tested samples. It can be observed that the value of the energy of thermal activation of conductivity decreases with the silver proportion increase. Also, with the increase of silver content, the value of the pre-exponential parameter also decreases.

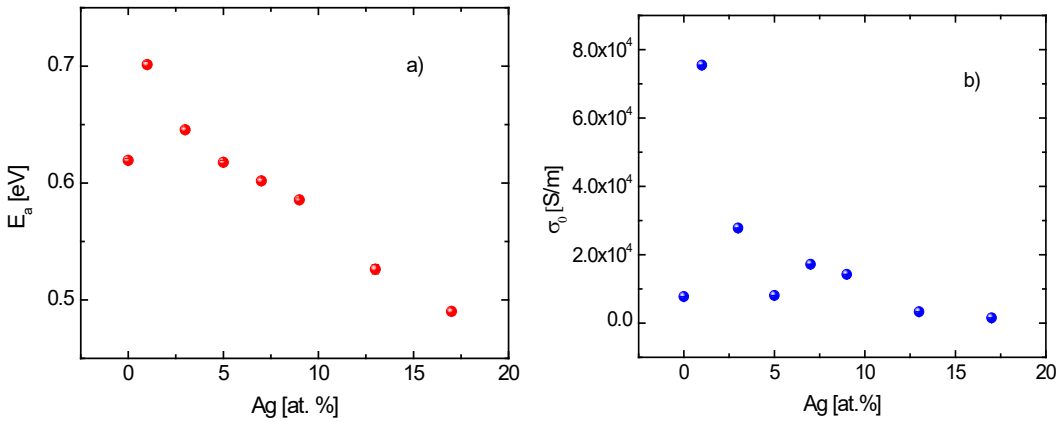

Fig. 6. The dependence of the activation energy (a) and the pre-exponential factor (b) on the proportion of silver in amorphous samples from the $Ag_x(As_2(Te_{0.5}Se_{0.5})_3)_{100-x}$ system.

According to the Davis and Mott criteria [31], the factor σ_0 should be between 10000 and 50000 S m^{-1} for most amorphous chalcogenides, in the case of hopping into delocalized states. Based on these findings, as well as the values obtained for thermally stimulated conduction, it can be concluded that the dominant mechanism for charge carrier transport in amorphous samples of the investigated composition within the studied temperature range involves hopping into delocalized states from localized states near the Fermi level. This occurs in the mobility gap, where the energy difference represents the gap between the delocalized states and the Fermi level, approximately corresponding to half the width of the forbidden zone. The decrease in activation energy results from the increased content of Ag+ ions involved in the transport of charge carriers [26]. DC conductivity tests on the chalcogenide material with sulfur (S) instead of tellurium (Te) revealed a similar trend of decreasing activation energy with increasing silver content. However, the changes observed in this system are notably larger. The activation energy decreases significantly from 0.895(16) eV in the composition with 1 at.% silver to 0.197(6) eV in the composition with 10 at.% silver. In the Ag-As-Se-Te system examined in this study, slightly lower activation energy values for DC conductivity - and consequently narrower forbidden zone widths - are expected compared to the Ag-As-Se-S system. This can be ascribed to the higher polarizability of the larger Te atoms compared to the smaller S atoms. Glasses composed of atoms with larger radii, which are more easily polarized, tend to exhibit narrower forbidden zones [32].

As can be seen from Table 1 and Figure 6b the introduction of a small amount of silver leads to the significantly higher values of the pre-exponential factor. As the proportion of silver increases, the pre-exponential factor decreases, indicating that silver gradually assumes control over the properties and the conductivity becomes more temperature-dependent, based on the data presented in Table 1, there is a noticeable decrease in the activation energy of the charge carriers.

Some applications of chalcogenide glasses leverage the significant difference in conductivity between their crystalline and amorphous phases. The first step in exploring this potential is determining the conductivity of samples subjected to thermally induced crystallization. To achieve this, the samples were annealed at their crystallization temperature, determined from DSC measurements [27], and held at this temperature for 30 minutes. Figure 7 illustrates the DC conductivity of the crystalline specimens.

As expected, the crystalline phase exhibited higher conductivity than the amorphous phase. However, the experiments also revealed some unexpected results. Notably, the conductivity of annealed samples decreased with increasing silver content. This may be ascribed to the introduction of silver, which increases the number of structural phases and defects, thereby reducing conductivity. Furthermore, the temperature had minimal impact on the conductivity of specimens with lower silver content. In contrast, specimens with 13% and 17% Ag displayed behavior, following the Arrhenius equation. From the Arrhenius dependence, the thermal activation energies of DC electrical conductivity were determined as 0.524 eV for 13 at.% Ag and 0.622 eV for 17 at.% Ag. The significant temperature dependence observed for 13 and 17 at.% Ag

seem to be related to the charge mobility in the sample volume, which is reduced by presence of various barriers and defects (phase separation, new phases). At higher temperatures, the energy of electric charge carriers energy is usually large enough to overcome the barriers and mobility of charge carriers increase.

Interestingly, the sample with 13 at.% silver exhibited a change in conduction character at the highest applied temperatures, where its DC conductivity became temperature-independent.

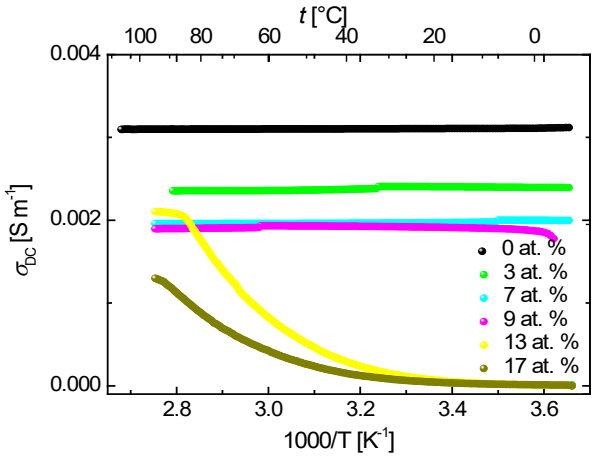

Fig. 7. DC conductivity in annealed samples from the $Ag_x(As_2(Te_{0.5}Se_{0.5})_3)_{100-x}$ system.

Figure 8 illustrates the changes in conductivity at 85°C with increasing silver content in both amorphous and thermally treated samples. For annealed samples containing 17 at.% silver, the conductivity increases by a factor of 3.8 compared to their amorphous counterparts. In the composition with 13 at.% silver, this increase is tenfold, while in the silver-free composition, the conductivity rises by approximately 74 times.

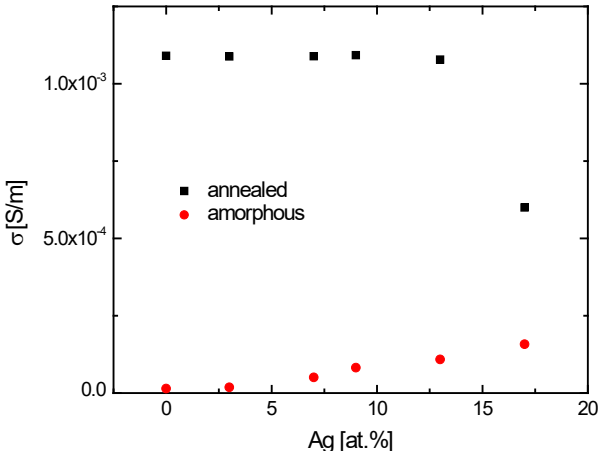

Fig. 8. A comparative analysis of the dependence of DC conductivity on the silver content for both amorphous and annealed samples in the $Ag_x(As_2(Te_{0.5}Se_{0.5})_3)_{100-x}$ system is presented.

4. Conclusion

In this study, the DC conductivity of amorphous and annealed samples from the $Ag_x(As_2(Te_{0.5}Se_{0.5})_3)_{100-x}$ system was investigated for x = 0, 1, 3, 5, 7, 9, 13, and 17 at.%. Crystallization in the annealed samples was thermally induced. Using a Scanning electron microscope, equipped with an energy dispersive spectrometer (EDS), the differences in the morphology of amorphous and annealed samples were confirmed. It was observed that in the annealed samples with a higher silver content, areas rich in silver appeared in the surface layer, which impacted the conductivity.

The DC conductivity measurements revealed that the amorphous samples exhibit semiconducting behavior, with conductivity increasing as the proportion of silver in the composition rises. At 85°C, the conductivity increases from $1.4678 \cdot 10^{-5}$ S/m for the silver-free composition to $1.5751 \cdot 10^{-4}$ S/m for the composition with 17 at.% silver. Electronic conductivity dominates, and percolation behavior begins to emerge at 7 at.% silver, with the conductivity exhibiting a mixed ionic-electronic character.

The thermal activation energy was derived from the Arrhenius dependence of conductivity on temperature, showing a decreasing trend with increasing silver content. The highest activation energy, 0.701(3) eV, was observed for the composition with 1 at.% silver, while the lowest, 0.490(3) eV, was found in the composition with 17 at.% silver. Based on the activation energy and the pre-exponential factor from the Arrhenius equation, the dominance of electronic conduction in delocalized states, originating from states localized near the Fermi level, was confirmed.

An increase in conductivity was observed in annealed samples compared to the amorphous ones. In annealed samples, conductivity decreased as the silver content increased, likely due to the formation of additional phases and defects in the structure. For annealed samples with up to 9 at.% silver, conductivity exhibited a weak temperature dependence, whereas for 13 and 17 at.% silver, conductivity followed the Arrhenius dependence.

Acknowledgements

The authors acknowledge financial support of the Provincial Secretariat for Higher Education and Scientific Research (Contract No. 003076409 2024 09418 003 000 000 001/2) through project “Novel chalcogenide materials for efficient transformation and use of energy”; of the Ministry of Science, Technological Development and Innovation (Contract No. 451-03-137/2025-03/200156) and the Faculty of Technical Sciences, University of Novi Sad through project “Scientific and Artistic Research Work of Researchers in Teaching and Associate Positions at the Faculty of Technical Sciences, University of Novi Sad 2025” (No. 01-50/295). O. Bošák and M. Kubliha have been supported by the Slovak Science Foundation, projects APVV DS-FR-19-0036, APVV 22-0146 and by the European Regional Development Fund, Research and Innovation Operational Programme, contract No. ITMS2014+: 313011W085.

The authors report there are no competing interests to declare.

References

[1] Z.H. Khan, S.A. Khan, F.A. Agel, N. A. Salah, M. Husain, Advances in Nanomaterials, Springer, New Delhi, 135 (2016); https://doi.org/10.1007/978-81-322-2668-0_4

[2] J. Heo, W. J. Chung, (2014), Rare-earth-doped chalcogenide glass for lasers and amplifiers Chalcogenide Glasses, Woodhead Publishing, Sawston, 347 (2014) https://doi.org/10.1533/9780857093561.2.347

[3] J. Schubert, M.J. Schoning, Y.G. Mourzina, A.V. Legin, Y.G. Vlasov, W. Zander,H. Luth, Sensors and Actuators B: Chemical 76(1-3), 327 (2001); https://doi.org/10.1016/S0925-4005(01)00616-5

[4] B. Fan, B. Xue, Z. Luo, X.H. Zhang, H. Ma, L. Calvez, Journal of the American Ceramic

Society 102(3), 1122 (2019); https://doi.org/10.1111/jace.15954
[5] R. Svoboda, D. Brandova, Journal of Alloys Compound 770, 564 (2019); https://doi.org/10.1016/j.jallcom.2018.08.150
[6] A. Zakery, S.R. Elliott, Journal of Non-Crystalline Solids 330(1-3), 1 (2003); https://doi.org/10.1016/j.jnoncrysol.2003.08.064
[7] Y. Liu, R. Golovchak, W. Heffner, O. Shpotyuk, G. Chen, H. Jain, Journal of Materials Chemistry C1(40), 6677 (2013); https://doi.org/10.1039/c3tc30975d
[8] Y. Wu, M. Meneghetti, J. Troles, J.L. Adam, Applied Sciences 8(9), 1637 (2018); https://doi.org/10.3390/app8091637
[9] N.A. Hegab, M. Fadel, I.S. Yahia, A. M. Salem, A.S. Farid, Journal of Electronic Materials 42(12), 3397 (2013); https://doi.org/10.1007/s11664-013-2756-z
[10] M.J. Schoning, J.P. Kloock, Electroanalysis 19(19-20), 2029 (2007); https://doi.org/10.1002/elan.200703955
[11] B.J. Eggleton, B. Luther-Davies, K. Richardson, Nature photonics 5, 141 (2011); https://doi.org/10.1038/nphoton.2011.309
[12] V.S. Vassilev, S.V. Boycheva, Talanta 67(1),20 (2005); https://doi.org/10.1016/j.talanta.2005.02.027
[13] M. Frumar, B. Frumarova, T. Wagner, Comprehensive Semiconductor Science and Technology, ed. by P. Bhattacharya, R. Fornari, H. Kamimura, Elsevier, Amsterdam, 206 (2011); https://doi.org/10.1016/B978-0-44-453153-7.00122-X
[14] Q. Yan, H. Jain, G. Yang, J. Ren, G. Chen, Journal of Applied Physics 112(5),053105 (2012); https://doi.org/10.1063/1.4752027
[15] T. V. Moreno, L.C. Malacarne, M.L. Baesso, W. Qu, E. Dy, Z. Xie, J. Fahlman, J. Shen, N. G. C. Astrath, Journal of Non-Crystalline Solids 495, 8 (2018); https://doi.org/10.1016/j.jnoncrysol.2018.04.057
[16] A.B. Seddon, Journal of Non-Crystalline Solids 184, 44 (1995); https://doi.org/10.1016/0022-3093(94)00686-5
[17] G. Yang, H. Jain, A. Ganjoo, D. Zhao, Y. Xu, H. Zeng, G. Chen, Optic Express 16(14), 10565 (2008); https://doi.org/10.1364/OE.16.010565
[18] B. Sujatha, N. Reddy, R. Chakradhar, Philosophical Magazine 20(19), 2635 (2010); https://doi.org/10.1080/14786431003662564
[19] M. Jabeen, N. Ali , Z. Ali, H. Ali, A. A. A. Bahajjaj, B. Haq, S.H. Kim, Chalcogenide Letters 21(2), 125 (2024); https://doi.org/10.15251/CL.2024.212.125
[20] S. Cui, C. Boussard-Pledel1, L. Calvez, F. Rojas, K. Chen, H. Ning, M.J. Reece, T. Guizouarn, B. Bureau, Advances in Applied Ceramics:Structural, Functional and Bioceramics 114(1), 42 (2015); https://doi.org/10.1179/1743676115Y.0000000054
[21] J. Zheng, L. Li, H. Yin, Y. Wang, J. Wei, H. Zeng, F. Xia, G. Chen, Ceramics International 46(14), 22826 (2020); https://doi.org/10.1016/j.ceramint.2020.06.050
[22] S. Stehlik, J. Kolar, M. Bartos, M. Vlcek, M. Frumar, V. Zima, T. Wagner, Solid State Ionics 181(37-38), 1625 (2010); https://doi.org/10.1016/j.ssi.2010.09.016
[23] Yu G. Vlasov, E.A. Bychkov, B.L. Seleznev, Solid State Ionics 24(3), 179 (1987); https://doi.org/10.1016/0167-2738(87)90158-5
[24] Yu G. Vlasov, E.A. Bychkov, B.L. Seleznev, Solid State Ionics 18-19(1), 467 (1986); https://doi.org/10.1016/0167-2738(86)90161-X
[25] F. Kyriazis, A. Chrissanthopoulos, V. Dracopoulos, M. Krbal, T. Wagner, M. Frumar, S.N. Yannopoulos,Journal of Non-Crystalline Solids 355(37-42), 2010 (2009); https://doi.org/10.1016/j.jnoncrysol.2009.04.070
[26] M. Krbal, T. Wagner, T. Srba, J. Schwarz, J. Orava, T. Kohoutek, V. Zima, L. Benes, S.O. Kasap, M. Frumar,Journal of Non-Crystalline Solids 353(13-15), 1232 (2007); https://doi.org/10.1016/j.jnoncrysol.2006.11.024
[27] R. Vigi, O. Bošák, D. Štrbac, G. Štrbac, Journal of Thermal Analysis and Calorimetry,

(2024); https://doi.org/10.1007/s10973-024-13253-x

[28] Z. Borisova, "Glassy Semiconductors", Springer Science+Business Media, New York, 393 (1981); https://doi.org/10.1007/978-1-4757-0851-6

[29] S. Stehlik, P. Knotek, T. Wagner, V. Zima, M. Bartos, S.O. Kasap, M. Frumar, Journal of Non-Crystalline Solids. 355(37-42),2054 (2009); https://doi.org/10.1016/j.jnoncrysol.2009.04.067

[30] K. O. Čajko, D. L. Sekulić, D. M. Petrović, V. Labaš, S. Minarik, S. J. Rakić, S. R. Lukić-Petrović,Journal of Non-Crystalline Solids 571,121056 (2021); https://doi.org/10.1016/j.jnoncrysol.2021.121056

[31] N. F. Mott, E. A. Davis, Electronic Processes in Non-Crystalline Materials Oxford University Press, New York 7 (1979)

[32] G. R. Štrbac, S. R. Lukić-Petrović, D. D. Štrbac, V. Benekou, A. Chrissanthopoulos, S. N. Yannopoulos, The Journal of Physical Chemistry B 124(14), 2950 (2020); https://doi.org/10.1021/acs.jpcb.0c00799